Eur. Phys. J. Appl. Phys. (2013) 64: 24512
DOI: 10.1051/epjap/2013120439

THE EUROPEAN PHYSICAL JOURNAL
APPLIED PHYSICS

Regular Article

Localization of metal targets by time reversal of electromagnetic waves*

3D-numerical and experimental study

Mehdi Benhamouche[1,2,a], Laurent Bernard[1], Mohammed Serhir[2], Lionel Pichon[1], and Dominique Lesselier[2]

[1] Laboratoire de Génie Electrique de Paris UMR 8507 CNRS, SUPELEC, Université Paris-Sud, UPMC, 11 rue Joliot-Curie, 91192 Gif-sur-Yvette Cedex, France
[2] Laboratoire des Signaux et Systèmes UMR 8506 CNRS, SUPELEC, Université Paris-Sud, 3 rue Joliot-Curie, 91192 Gif-sur-Yvette Cedex, France

Received: 2 October 2012 / Received in final form: 22 December 2012 / Accepted: 16 April 2013
Published online: 6 November 2013 –

Abstract. This paper proposes a criterion for locating obstacles by time reversal (TR) of electromagnetic (EM) waves based on the analysis of the density of EM energy map in time domain. Contrarily to a monochromatic study of the TR, the wide-band approach requires to determine the instant of the wave focus. This enables us to locate the focal spots that are indicative of the positions. The criterion proposed is compared to the inverse of the minimum entropy criterion as used in the literature [X. Xu, E.L. Miller, C.M. Rappaport, IEEE Trans. Geosci. Remote Sens. **41**, 1804 (2003)]. An application for the localization of 3D metal targets is proposed using finite integration technique (FIT) as computational tool at the modeling stage. An experimental validation is presented for canonical three-dimensional configurations with two kinds of metal objects.

1 Introduction

The analysis of wave propagation is widely used in imaging and environment characterization using waves of different nature (acoustic, EM, elastic) [2–5].

In the late 1980s, Fink et al. [6] have introduced the time reversal (TR) notion in an ultrasonic acoustic context. In the early 1990s, the study of this phenomenon has been extended by the same scientists using the decomposition of the TR operator (DORT in its French acronym). TR is based on the time invariance of the wave equation in non-dissipative media. The first experimental device confirming this phenomenon has been set up by Derode et al. [7]. The authors show the ability of acoustic waves, crossing a random strongly scattering medium, to return to their original source. The device is essentially based on the installation of a time reversal mirror (TRM, called also TR Array) using piezo-electric transducers.

TR principle was then successfully extended to electromagnetic (EM) waves. Tortel et al. [8] initiated the 2D EM monochromatic study of TR for dielectric cylinders and perfectly conducting ones in free space. They use DORT to study the effect of the TRM polarization and object geometries on the localization. The authors show, based on numerical results, the efficiency of DORT in the selective imaging with EM waves and in the identification of small separate dielectric objects (when the distance between them is more than one third of the local wavelength).

Among the first works in the time domain, there are those presented by Yavuz and Teixeira [9] and those published by Kosmas et al. [10], both on 2D configurations. Probably because of the complexity of Green's integrals in heterogeneous media and the high cost of their evaluation on a large frequency band, the study is carried out numerically using the technique of finite differences (FD) in time domain.

Notice that many applied mathematical works on imaging of obstacles including TR under various forms exist in the literature, refer to the forthcoming book [11]. Also, a recent contribution on 3D electromagnetic TR [12] shows how TR with properly band-limited pulses enables some refocusing onto the position of a small scatterer. Questions of effects of dispersion and attenuation in the host medium on the efficiency of TR localization remain open however.

TR is mainly applied for telecommunications [13,14] and imaging [10,15,16] purposes. We propose in this work a model of the TR-EM-wave for target localization using the finite integration technique (FIT). Since our study of

* Contribution to the Topical Issue "Numelec 2012", Edited by Adel Razek.

[a] e-mail: mehdi.benhamouche@supelec.fr

TR is led in the time domain, it is necessary to determine a field distribution that allows us to locate objects [17]. There are two methods in the literature to determine this distribution. The first method consists in taking advantage of the causality of the incident field on the scattered field. Indeed, the major wave fronts of the incident field, moving in reverse chronology, intersect with those of the returned field (obtained by the back-propagation of the scattered field) at the object location. The scatterer's location matches with maximum of the convolution between the incident field and returned field [18].

The second method involves determining the instant of focus by analyzing the evolution of the returned field distribution, at the back-propagation step. This gives the appropriate distribution of field from which the location of the scatterers can be inferred.

Both methods require the calculation of the field (or density of EM energy) on a grid of points in the search area (where the location of scatterer is expected). The first type of method requires, in addition, the knowledge of the spatio-temporal evolution of the incident fields in the search area (calculated on the grid). Otherwise it is simply impossible to use. In our study we focus on the second method and we try to combine with the first one in some cases to exploit the best of their advantages.

2 Localization methods

Maxwell's equations are time-symmetric, so a TR electromagnetic field is expected to go back toward the sources. Since an obstacle illuminated by a given EM wave can be considered as a set of secondary sources within it (or on its surface), the TR of the scattered field must converge toward the obstacle (in some sense, to be considered further) [17].

2.1 Evaluation of the instant of focus

In a given time interval during the back-propagation, the EM energy density ρ is calculated on a homogeneous grid of a rectangular parallelepiped search area. A time interval I is chosen so that the major wave fronts propagate through the whole search area. At a given instant $t_i \in I$ we define the class S_k, $k \in [|1,\, K|]$, according to the value of the EM energy density ρ_j at each point n_j, as follows:

$$n_j \in S_k \Leftrightarrow \frac{K-k}{K}\rho_{\max} < \rho_j \leq \frac{K-k+1}{K}\rho_{\max}. \quad (1)$$

Then we note $N_k = |S_k|$, $k \in [|1,\, K|]$ as the cardinality of the set S_k. For a given number of classes K, we associate the following function:

$$\Phi_K : t_i \longmapsto \Phi_K(t_i) = \sum_{k=1}^{K} \frac{kN_k(t_i)}{KN}, \quad (2)$$

$N = \sum_{k=1}^{K} N_k$ is the number of points n_j in the grid G. This function represents the summation of normalized volumes $\frac{N_k(t_i)}{N}$, linearly weighted by $\frac{k}{K}$, at the instant t_i. Its overall shape does not depend on the choice of K and one can deduce, using formula (1), that for all t_i,

$$\lim_{K \longrightarrow +\infty} \Phi_K(t_i) = \Phi_\infty(t_i) = 1 - \frac{\sum_{j=1}^{N} \rho_j(t_i)}{N\rho_{\max}(t_i)}. \quad (3)$$

The instant of focus is given by

$$t_f = \arg\max_{t_i} \Phi_\infty(t_i). \quad (4)$$

This procedure can be interpreted as finding the point where the volumes of regions of low energy density are the largest, while remaining in a time interval where the energy is mainly in the search area. From (3), we note that $\Phi_\infty(t)$ behaves like $-\frac{E_n(t)}{\rho_{\max}(t)}$, where $E_n(t) = \frac{E(t)}{\max_{t\in I} E(t)}$ is the normalized EM energy in the search area. The inverse of minimum entropy criterion [10] is denoted ψ, where the square of the electric field is replaced by the density of the EM energy:

$$\psi(t) = \frac{\sum_{j=1}^{N} \rho_j(t)^2}{\left(\sum_{j=1}^{N} \rho_j(t)\right)^2}. \quad (5)$$

If we note $\psi_p(t) = \frac{\left[\sum_{j=1}^{N} \rho_j(t)^{p+1}\right]^{\frac{2}{p+1}}}{\left[\sum_{j=1}^{N} \rho_j(t)^{p}\right]^{\frac{2}{p}}}$, the link between the two criteria is given by

$$\Phi_\infty = 1 - \frac{1}{N}\left[\prod_{p=1}^{\infty} \psi_p\right]^{-\frac{1}{2}}. \quad (6)$$

2.2 Causality incident-scattered field

When the spatio-temporal distribution of the incident field is known or can be calculated, a localization method based on causality can be used. The scattered field is caused by the incident field in the presence of scattering objects. In the time domain, pulses of the scattered field appear when the incident field comes into contact with the scatterers. Therefore, if the objects are not located between the source of excitation and the TRM, the intersection between the incident field propagating in reverse chronology and the field returned by the TRM can give the location of the scatterers [18].

The procedure is simple, if $\rho_j^{\text{inc}}(t)_{t\in[0\,T]}$ and $\rho_j^{rt}(t)_{t\in[0\,T]}$ are, respectively, the densities of the EM energy corresponding to the incident fields and fields back-propagated by the TRM calculated at a point p_j of grid G, the convolution

$$\text{Conv}_j = \int_{[0\,T]} \rho_j^{\text{inc}}(T-t)\rho_j^{rt}(t)\,\mathrm{d}t, \quad (7)$$

exhibits local maxima at the positions of scatterers.

It is not advisable to apply this method in case of transmission, when the targets (objects) are located between the source of excitation and the TRM. It also cannot be applied for the localization of primary sources.

3 Localization of two spheres (all numerical)

3.1 Numerical Model

For solving wave problems in time domain, FD is often used as a numerical model in the literature because of its ease of implementation and its moderate requirement in terms of machine performance. On the contrary, finite elements (FE) and finite volumes (FV) in time domain methods are less popular because of their implicit nature at least when dealing with TR. Here, we use the FIT which is as a general framework for FD and FE methods.

Introduced by Weiland [19], the FIT method, also known as the generalized FD [20] or cell method [21], consists in discretizing Maxwell's equations in their integral form. The EM quantities (induction fluxes and field circulations) are discretized on the cells (faces, edges) of two dual meshes. Constitutive matrices make the relation between fluxes and circulations taking into account the geometry of the meshes and the material properties. The FIT is equivalent to the FD method when applied to the orthogonal grid mesh type, but it also allows to use unstructured meshes in the manner of the FE method [22]. The basic algebraic properties of this theory of discretization of Maxwell's equations can prove, analytically and algebraically, energy and charge conservation. Such algebraic properties then enable the development of numerical schemes that ensure long-term stability during the resolution in the time domain [23].

In our study, unstructured meshes are used to model the direct problems (incident and scattered fields) in order to finely take into account the geometry of the targets. Orthogonal grids are used to model the inverse problem (back-propagation of the scattered field) in which there is no target.

In each cell (c) of the primal mesh, the density of electromagnetic energy is evaluated by:

$$\rho_c = \frac{1}{v_c}\frac{1}{2}\left(e_c^t \epsilon_c e_c + b_c^t \nu_c b_c\right), \tag{8}$$

where v_c is the volume of the cell, e_c and b_c are respectively the vector of electric field circulation along the edges of the cell and the vector of magnetic induction flux through the faces of the cell, ϵ_c and ν_c are the permittivity and reluctivity constitutive elemental matrices.

Let us consider two perfectly electrically conducting spheres with the same radius 0.1 m centered respectively at coordinates (−0.27 m, 0.17 m, 0.36 m) and (0.28 m, 0.17 m, −0.17 m). They are illuminated by an electric dipole polarized along the x-axis centered on the rectangular plane located at $y = 1.83$ m defined by its diagonal ends (1.58 m, 1.83 m, 1.6 m) and (−1.58 m, 1.83 m, −1.50 m). This surface serves as a support for the TRM composed of 9×9 x-polarized dipoles (edges of the mesh), Figure 1.

The computational domain is a rectangular parallelepiped (each face is parallel to one of the planes: $x = 0$, $y = 0$ or $z = 0$) defined by the ends of its space diagonal (−1.58 m, −0.42 m, −1.58 m) and (1.58 m, 1.83 m, 1.67 m). It is divided into 36 subdomains separated by layers of cubes and prisms in order to make the constitutive matrices block-diagonal. This eases the factorization and subsequently solving linear systems involved in the time stepping scheme. The whole domain is surrounded by perfectly matched layers (PML) in order to simulate the infinite space [24]. Note that the space discretization is 0.083 m, so one has 13 nodes per meter. The time step is taken as the ratio of the smallest edge of the mesh to 12 times the speed of light in the vacuum, or $\mathrm{d}t = 1.14\times10^{-11}$ s in order to ensure stability. The electromotive force V_s applied to the excitation dipole is a modulated Gaussian pulse defined by

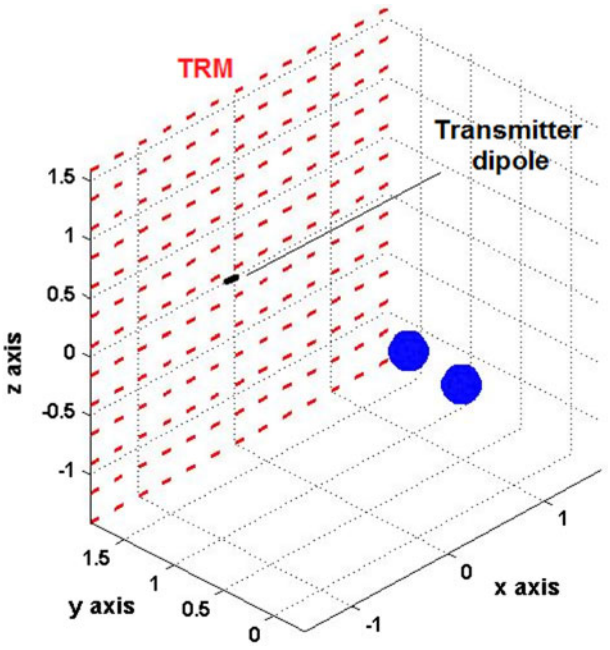

Fig. 1. 3D view of the configuration.

$$V_s = \cos(2\pi f_m(t - t_0))\exp(-(4c_0(t - t_0))^2), \tag{9}$$

its spectrum being depicted in Figure 2.

The TR process consists of four steps: (1) illuminating the spheres by the modulated Gaussian propagating

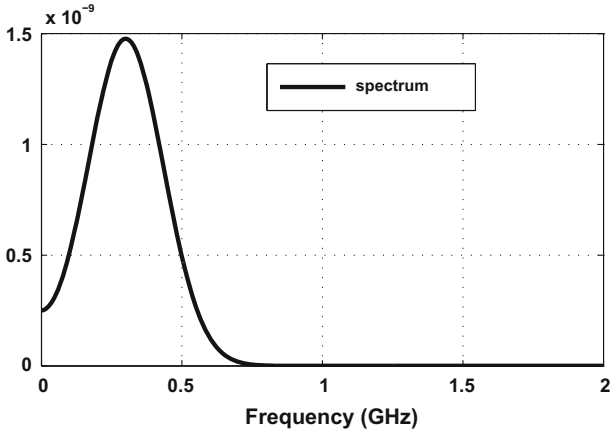

Fig. 2. Spectrum of the modulated Gaussian pulse.

source pulse, (2) recording the scattered field on an array (TRM) of electric dipoles, (3) using this TRM to emit the recorded signals (chronologically reversed) in free space, using an orthogonal mesh as a support of discretization, (4) getting an image of the field distribution when focusing occurs. The search domain is also a rectangular parallelepided defined by the two points (−1.58 m, −2.42 m, −1.58 m) and (1.58 m, 1.65 m, 1.67 m) forming its diagonal. Here, the point grid on which the EM energy density is calculated consists of the cell barycenters located in the search area. We perform the calculation of $\Phi_\infty(t)$ and $\psi(t)$ in the interval $\left[\frac{6.3}{c_0}, \frac{8.2}{c_0}\right]$ and we look for the times corresponding to their respective maxima, Figure 3.

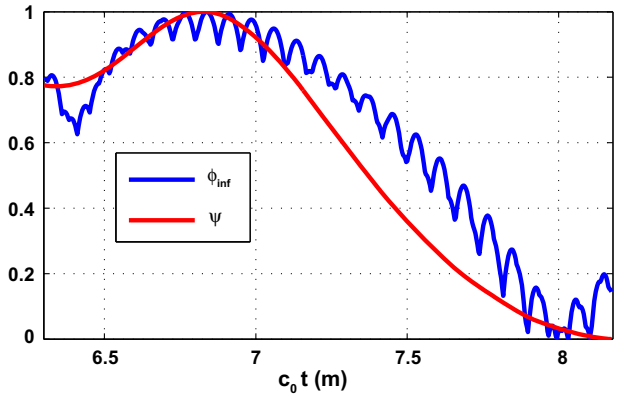

Fig. 3. Behavior of $\Phi_\infty(t)$ and $\psi(t)$ normalized in the interval $\left[\frac{6.3}{c_0}, \frac{8.2}{c_0}\right]$ in the interval [1, 0].

The instants of focus found by Φ_∞ and ψ are the same $t_\psi = t_\phi = \frac{6.8}{c_0}$ s. The period of oscillation of Φ_∞ is related to the distance between two neighbor points of the grid. For example, in the interval $\left[\frac{7}{c_0}, \frac{7.5}{c_0}\right]$, we can see six oscillations of Φ_∞, Figure 3. The spatial period of oscillation is $\frac{7.5-7}{6} = 0.083$ m which is exactly the size of the edges of the mesh. In consequence, the resolution localization cannot be less than 0.083. That is why we keep only one digit values of $c_0 t$. The distribution of the normalized EM energy density is plotted in the planes $x = -0.27$ m, $x = 0.28$ m, $z = -0.17$ m and $z = 0.36$ m at time t_ϕ, Figure 4.

For both spheres, the focal spots are located at the faces exposed to the TRM. Note that the focal spots are more visible and clearer in the x planes (perpendicular to the TRM dipoles) as seen in Figure 4. In the plane parallel with the direction of polarization of the dipoles, the focus is less visible but the results are globally satisfactory. The use of bipolar dipoles (cross-shaped along x- and z-axes) in the TRM leads to similar results as those presented in this example. Indeed, the EM field returned by the dipoles oriented along the axis z is very small compared to those returned by the x-axis oriented dipoles. As the distribution of the density of EM energy (which depends on the square fields) is studied, the contribution of the z-axis oriented dipoles is even more negligible. Nevertheless, the use of cross-polarized dipoles in the TRM is necessary if one ignores the polarity of the transmitter dipole or the nature of the objects that could be depolarizing. The convolution method is then applied in the x and z planes crossing the spheres, Figure 5. The results are very similar to those obtained by the focus instant method.

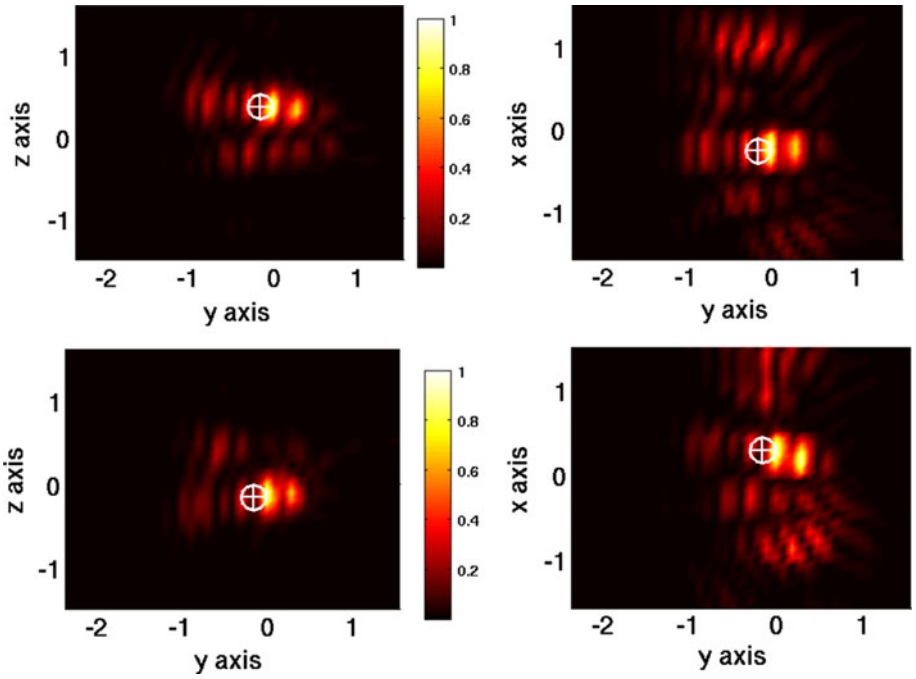

Fig. 4. Normalized density of EM energy computed in the x and z planes crossing the centers of the two spheres.

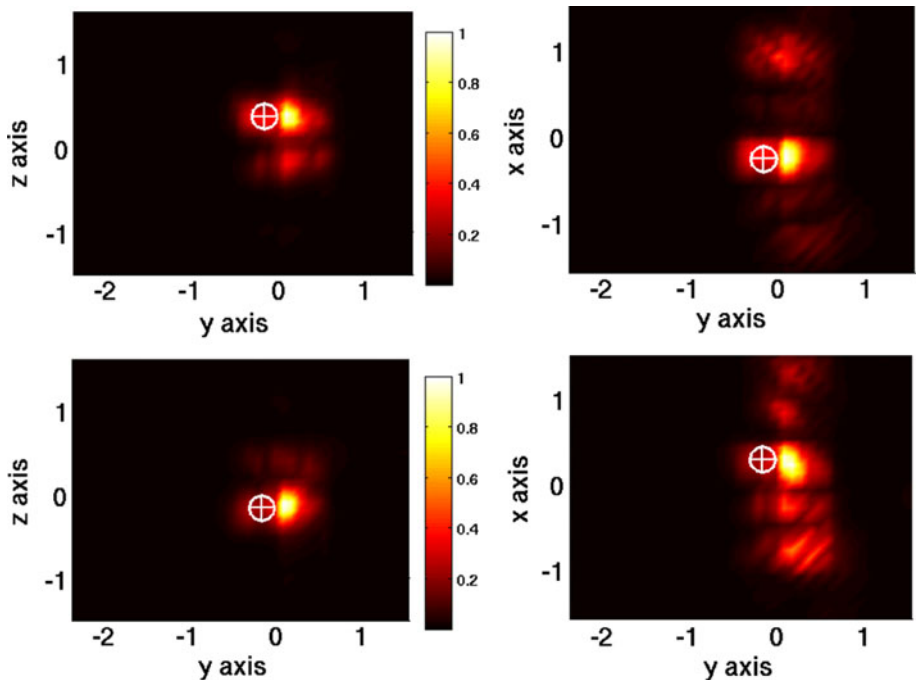

Fig. 5. Normalized convolution computed in the x and z planes crossing the centers of the two spheres.

4 Localization of a metal stem and plate (experimental and numerical)

4.1 Experimental device

The efficiency of the approach is checked through an experimental validation. In order to respect the free space propagation conditions, we carry out the experimental measurements in an anechoic chamber. We generate a pulsed EM incident field using a wide-band [0.5 GHz, 9 GHz] horn antenna excited by a step signal pulse. This antenna radiates a pulsed electric field which is linearly polarized along the y-axis and propagates in the direction $-z$ (toward the target). Behind the target, we place a sensor (probe) which collects the y-electric field component in the frequency band [0.3 MHz, 3 GHz]. In the presence of the target to be characterized, we move the linearly polarized probe on a regular grid to measure the total field radiated in the time domain, Figure 6.

The total field results from the incident field coming from the antenna and the field scattered by the target. The signal measured by the probe is transmitted via an optical fiber to the sampling oscilloscope. For our experiment the considered grid consists of 9×9 measurement positions in a rectangular surface in the plane $z = 0$. The diagonal ends of this surface are given by (-0.6 m, -0.6 m, 0 m) and (0.6 m, 0.6 m, 0 m).

In our experimental procedure, we are specifically interested in the field scattered by the target. We initially measure the incident field in the absence of the metal target. In a second step, we measure the total field in the presence of the target. The scattered field is the difference between the total and incident field. This procedure is repeated for two different metal targets: a stem and a plate respectively characterized by the following dimensions $1.6 \times 23 \times 1.6$ cm and $19 \times 15.9 \times 0.1$ cm.

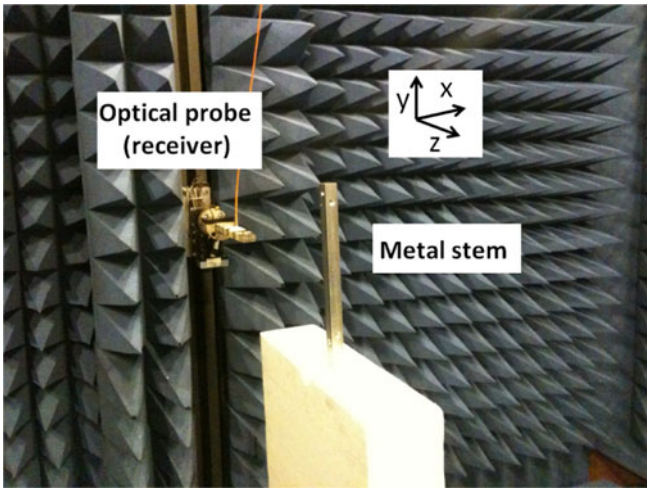

Fig. 6. Scatterer and reception device.

The two targets are placed at 0.6 m from the aperture of the antenna and the probe moves along a rectangular grid located at 1 m from the target. To improve the measurement accuracy, the data recorded by the oscilloscope are averaged and digitally filtered to minimize the measurement noise.

The pulses, corresponding to the field scattered by the objects, are time reversed and injected into the numerical model using electric dipoles polarized as the pulsed electric field transmitted by the horn antenna. The electric field, at a given instant, is assumed constant along each electric dipole represented by an edge of a mesh element.

The dipoles forming a TRM are placed in a surface where the probe moves to collect the electric field.

4.2 Discussion

As it is presented, the two criteria are compared and give similar results in both configurations, at least for this choice of dipole density in the TRM, Figures 7 and 8. They correspond to the instant when the wave fronts start diverging (post-focusing), in both configurations. The obtained instants of focus well verify the two criteria for the case of the stem. In the case of the plate, ϕ_∞ and ψ do not reach their global maximum when the main wave front focuses on the object. This is due to the high level of noise that can be seen in Figure 10. However, ϕ_∞ and ψ represent a local maximum at this instant. In consequence, the correct instant of focus can only be deduced by a careful interpretation of the evolution of the two functions. Indeed, the instant of focus matches with the instant of the last significant local maximum which defines the beginning of the divergence period. For each object, there is a focal spot of high intensity near the surface exposed to the TRM, Figures 9 and 10. This allows to find the location of each target.

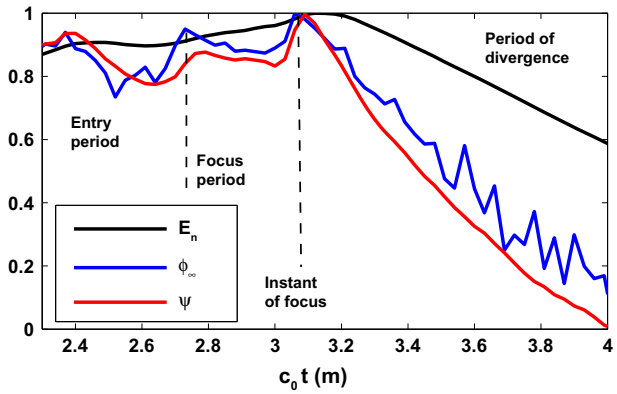

Fig. 7. Behavior of the criteria, case of the stem.

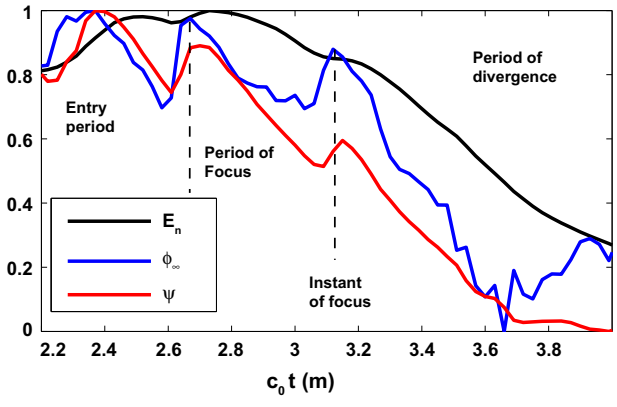

Fig. 8. Behavior of the criteria, case of the plate.

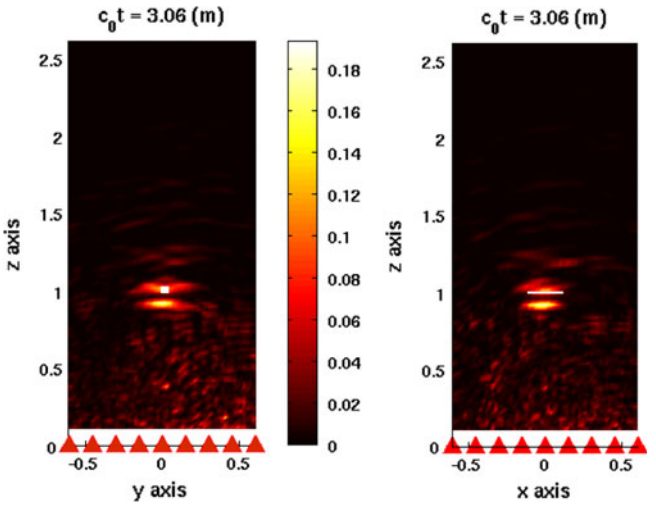

Fig. 9. Distribution of the normalized density of EM energy at the instant of focus $c_0 t_f = 3.06$ m (stem).

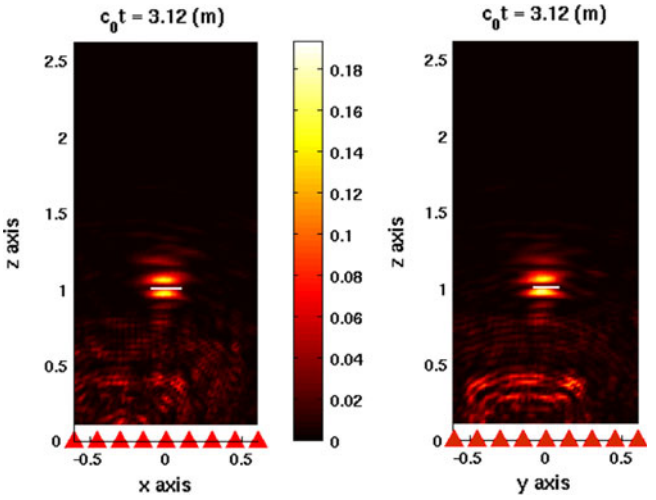

Fig. 10. Distribution of the normalized density of EM energy at the instant of focus $c_0 t_f = 3.12$ m (plate).

5 Conclusion

Through this work, we can see the usefulness of the FIT method in TR modeling steps. Indeed, it allows the use of unstructured grids to properly model the curvatures of the objects when calculating the direct problem, and to use orthogonal grid mesh type in the back-propagation step where there are no objects and where the computational performance is required (high speed and more memory needed). A new criterion is introduced in this paper for determining the instant of returned wave focus. This method is another way to choose the distribution of the EM energy density which corresponds to the instant of focus.

The whole localization process is based on a time-domain wide-band approach and is shown to be efficient thanks to experimental and numerical tests on metal

objects. In particular, it gives results comparable to those obtained by the causality method while it does not require the computation of the incident field nor any convolution product. It also makes it possible to localize primary sources which could be useful for example in an electromagnetic compatibility context to identify parasitic radiating sources.

One can see that the inverse of minimum entropy criterion behaves as a ratio of norms $\frac{l^2(\rho)}{l^1(\rho)}$ of a given distribution ρ and the criterion introduced behaves as a ratio of norms $\frac{l^\infty(\rho)}{l^1(\rho)}$. So we deduce that we could also use a criterion which behaves like $\frac{l^p(\rho)}{l^1(\rho)}$ where $2 \leq p \leq \infty$. The interest to use these two extreme criteria (compared in models and in experiments) is to confirm the instant of focus or the beginning of the TR wave divergence.

References

1. X. Xu, E.L. Miller, C.M. Rappaport, IEEE Trans. Geosci. Remote Sens. **41**, 1804 (2003)
2. H. Ammari, P. Garapon, L. Guadarrama Bustos, H. Kang, J. Differ. Equ. **249**, 1579 (2010)
3. H. Ammari, J. Garnier, K. Sølna, Waves in Random & Complex Media **22**, 40 (2012)
4. K.J. Langenberg, K. Mayer, R. Marklein, Cem. Conc. Comp. **28**, 370 (2006)
5. K.J. Langenberg, K. Mayer, A. Zimmer, Nondestructive evaluation of embedded structures in concrete: modeling and tomographic imaging, in *URSI EMTS, Pisa, Italy, 2004*
6. M. Fink, D. Cassereau, A. Derode, C. Prada, P. Roux, M. Tanter, J.-L. Thomas, F.Wu, Rept. Progr. Phys. **63**, 1933 (2000)
7. A. Derode, P. Roux, M. Fink, Phys. Rev. Lett. **75**, 4206 (1995)
8. H. Tortel, G. Micolau, M. Saillard, J. Electromagn. Waves Appl. **13**, 687 (1999)
9. M.E. Yavuz, F.L. Teixeira, IEEE Antennas Wirel. Propag. Lett. **4**, 43 (2005)
10. P. Kosmas, C.M. Rappaport, E. Bishop, IEEE Trans. Microwave Theor. Tech. **52**, 1890 (2004)
11. H. Ammari, M.S. Vogelius, D. Volkov, Journal de Mathématiques Pures et Appliquées **80**, 769 (2001)
12. S. Gdoura, A. Wahab, D. Lesselier, J. Phys.: Conf. Ser. **386**, 012010 (2012)
13. S.-Q Xiao, J. Chen, B.-Z. Wang, X.F. Liu, PIER **1**, 329 (2007)
14. M. Davy, M. De Rosny, J.-C. Joly, M. Fink, C. R. Phys. **11**, 37 (2010)
15. N. Maaref, P. Millot, X. Ferrières, C. Pichot, O. Picon, PIER **1**, 59 (2008)
16. L. Bellomo, K. Belkebir, M. Saillard, S. Pioch, P. Chaumet, Inverse scattering using a time reversal RADAR, in *2010 URSI International Symposium on Electromagnetic Theory (EMTS), Berlin, Germany, 2010*, pp. 381–384
17. M. Benhamouche, L. Bernard, L. Pichon, D. Lesselier, IEEE Trans. Magn. **48**, 359 (2012)
18. M. Neyrat, PhD thesis, Faculté des Sciences et Techniques XLIM – Département OSA, Université de Limoges, France, 2009
19. T. Weiland, I. Munteanu, State of the art and future in modeling RF components, in *EuCAP 2006, Nice, France, 2006*, p. 6.1
20. A. Bossavit, PIER **32**, 45 (2001)
21. M. Marrone, PIER **32**, 317 (2001)
22. L. Bernard, L. Pichon, Eur. Phys. J. Appl. Phys. **52**, 23307 (2010)
23. M. Clemens, T. Weiland, PIER **32**, 65 (2001)
24. L. Bernard, R.R. Torrado, L. Pichon, IEEE Trans. Magn. **46**, 3492 (2010)